

# Free-carrier screening of polarization fields in wurtzite GaN/InGaN laser structures

Fabio Della Sala,<sup>1</sup> Aldo Di Carlo,<sup>1</sup> Paolo Lugli,<sup>1</sup> Fabio Bernardini,<sup>2</sup> Vincenzo Fiorentini,<sup>2,3</sup> Reinhard Scholz,<sup>4</sup> and Jean-Marc Jancu<sup>5</sup>

(1) INFM – Dipartimento di Ingegneria Elettronica, Università di Roma “Tor Vergata”, Roma, Italy

(2) INFM – Dipartimento di Fisica, Università di Cagliari, Italy

(3) Walter Schottky Institut, TU München, Garching, Germany

(4) Institut für Physik, TU Chemnitz, Germany

(5) INFM-Scuola Normale Superiore, Pisa, Italy

(9 September 1998)

The free-carrier screening of macroscopic polarization fields in wurtzite GaN/InGaN quantum wells lasers is investigated via a self-consistent tight-binding approach. We show that the high carrier concentrations found experimentally in nitride laser structures effectively screen the built-in spontaneous and piezoelectric polarization fields, thus inducing a “field-free” band profile. Our results explain some heretofore puzzling experimental data on nitride lasers, such as the unusually high lasing excitation thresholds and emission blue-shifts for increasing excitation levels.

42.55.Px, 71.15.-m, 71.20.Nr, 78.30.Fs, 78.60.-b

One of the major recent breakthroughs in semiconductor physics is the realization of blue lasers based on III-V nitride heterostructures technology [1,2]. In this area, several puzzling issues remain unsettled: *a*) the exact mechanism responsible for laser action is still a matter for debate [3,4]; *b*) unusually high threshold densities are required for laser action to occur (typically  $\sim 10^{13}$  cm<sup>-2</sup> vs  $\sim 10^{12}$  cm<sup>-2</sup> for GaAs based devices) [2,5,6]; *c*) a blue shift of the transition energy is observed for increasing excitation powers [7,8]; *d*) a red shift of the transition energy is observed for increasing well width.

In this Letter, we identify the central reason for these unusual behaviors, namely the interplay of free-carrier screening and macroscopic polarization fields. A peculiarity of wurtzite nitrides is that of having a non-zero macroscopic polarization, comprising both a spontaneous and a piezoelectric component [9]. The former is a property of low-symmetry materials in their ground state, is independent of strain, and is absent in zincblende materials (e.g. GaAs). The latter appears in the presence of strain, due to e.g. epitaxy. In III-V nitrides, both components are very large [9]; piezoelectric coupling, in particular, is orders of magnitude larger than in e.g. GaAs. In nitride multilayers, polarization manifests itself as large ( $\sim 1$  MV/cm) built-in electrostatic fields [10], produced by the charge related to polarization changes across heterointerfaces. The field-induced linear bending of the band edges causes a spatial separation of confined electrons and holes within the active layers of the devices [10,11], and has therefore important consequences on the optical properties of nitride-based LED’s or lasers.

Recent theoretical studies have predicted a reduced recombination rate in both GaN/InGaN [3] and AlGaIn/GaN [12] quantum wells for increasing well width, due to the field induced separation of electron and holes. Based on those results, it was argued that electron-hole recombination should be severely hindered, and that al-

ternative explanations of lasing, such as e.g. quantum dot formation, should be sought for. However, the results in question are not self-consistent, i.e. they neglect the presence of free electrons and holes in the quantum well. Here we show instead that self-consistent free-carrier screening is the key to understanding the effects of polarization fields on laser action in nitride devices.

Specifically, we investigate a prototypical nitride-based device, namely a single In<sub>0.2</sub>Ga<sub>0.8</sub>N quantum well pseudomorphically strained to the surrounding GaN barriers. To account for screening effects, we use the self-consistent tight-binding (TB) approach [13] which enables us to describe polarization fields, dielectric screening, and free-carrier screening in a fully self-consistent and non-perturbative way. TB is used in order to describe the electronic structure [13] in the whole Brillouin zone up to several eV’s above the fundamental gap, overcoming all the natural limitations of simple envelope function schemes. We use an  $sp^3d^5s^*$  TB Hamiltonian [14] representing the state-of-art of empirical TB; its parameters have been determined fitting the DFT-LDA band structure as outlined in Ref. [14]. A valence band offset of 0.106 eV is considered. [3] The self-consistent calculation is performed as follows. The electron and hole quasi-Fermi levels are calculated for a given areal charge density ( $n_{2D}$ ) in the quantum well (the *sheet density*, related to the injection current), and the electron ( $n$ ) and hole ( $p$ ) charge distributions in the nanostructure are obtained [13]. (The integrated hole and electron charges are equal, since charge neutrality is assumed). We then solve Poisson equation,

$$\frac{d}{dz}D = \frac{d}{dz} \left( -\varepsilon \frac{d}{dz}V + P_T \right) = e(p - n). \quad (1)$$

The (position-dependent) quantities  $D$ ,  $\varepsilon$ , and  $V$ , are respectively the displacement field, dielectric constant, and

potential. The (position-dependent) transverse polarization  $P_T$  is the sum of the spontaneous component  $P_s$ , calculated ab initio [9], and of the piezoelectric component  $P_{pz} = 2e_{31}\epsilon_{xx} + e_{33}\epsilon_{zz}$ , involving the calculated [9] piezoelectric constants  $e_{31}$  and  $e_{33}$ , and the strain tensor components  $\epsilon_{xx}$  and  $\epsilon_{zz}$ . These are obtained via elasticity theory in terms of the barrier ( $a_b$ ) and well ( $a_w$ ) lattice parameters [9] and elastic constants as  $\epsilon_{xx} = (a_b - a_w)/a_w$  and  $\epsilon_{zz} = -2\epsilon_{xx}C_{13}/C_{33}$ . The constants used in the calculation are listed in Table I. The spontaneous polarization and piezoelectric constants in the alloy region are obtained by interpolation according to Vegard's rule. The polarization change across the GaN/InGaN interface is  $0.0325 \text{ C/m}^2$ , corresponding to a bare interface polarization charge of  $2 \cdot 10^{13} \text{ cm}^{-2}$ . The resulting electrostatic field in the well, including dielectric screening but no free-carrier screening, is  $3.25 \text{ MV/cm}$ .

Poisson's equation is solved assuming zero field at the boundary. The potential thus obtained is plugged into the TB Schrödinger equation, which is solved to obtain energies and wavefunctions. The new quasi-Fermi levels are then calculated, and the procedure is iterated to self-consistency. No analytic approximation is made for the band dispersions; to calculate the charge density, a numerical  $k_{\parallel}$  integration is performed. Room temperature is assumed throughout all calculations.

Both the sheet carrier density and well width are varied in our calculations. This is of interest since it has been shown that the sheet density necessary to achieve lasing in InGaN/GaN laser structures is unusually large for typical semiconductor lasers [2,5,6]. The well width is also an important parameter in these structures since the total potential drop across the structure is directly proportional to the product of polarization field and well width, if free-carrier screening is neglected. Indeed, as mentioned earlier, it has been argued that structures with well width above than  $50 \text{ \AA}$  should not be able to produce laser action [3].

The first result concerns the conduction band profile of a  $100 \text{ \AA}$  InGaN well, shown in Fig. 1 for several sheet densities. For a relatively substantial sheet density,  $n_{2D} = 5 \cdot 10^{12} \text{ cm}^{-2}$ , a practically uniform electrostatic field as large as  $2.5 \text{ MV/cm}$  is still present in the well. By increasing the sheet density (i.e. the injection current), free-carrier induced screening becomes more and more efficient. Upon reaching  $n_{2D} = 5 \cdot 10^{13} \text{ cm}^{-2}$  a quasi-field-free shape of the quantum well is recovered. This is easily understood from the charge densities displayed in Fig. 2 at two typical sheet densities. Electrons and holes are indeed spatially separated by the polarization field, but the free-carrier-induced field is opposite to the polarization field. The two fields tend to cancel each other out for high sheet densities, thus reestablishing the conditions for electron-hole recombination emission.

In Fig. 3 we present the calculated transition energy between the highest hole level ( $V1$ ) and the lowest elec-

tron level ( $C1$ ), and the overlap of the  $C1$  and  $V1$  wavefunctions; the square of the overlap is proportional to the recombination rate between the two levels [15]. As seen in Fig. 3, upon increasing the sheet density we observe a blue shift in the transition energy and an increased recombination rate. This is due to the progressive recovery of flat band conditions upon increasing the sheet density. In addition, the recombination rate tends to saturate to a finite value at high sheet densities, and is therefore not vanishingly small for normal laser operation conditions (high free-charge density) as previously claimed [3]. (The difference in recombination rate at different well widths decreases with increasing sheet density: the recombination rate ratio for widths of  $25 \text{ \AA}$  and  $50 \text{ \AA}$  increases from  $3 \cdot 10^{-4}$  to  $0.1$  by increasing the sheet density from  $5 \cdot 10^{12} \text{ cm}^{-2}$  to  $5 \cdot 10^{13} \text{ cm}^{-2}$ .)

We conclude that laser emission can occur via direct electron-hole recombination without having to invoke composition fluctuations and dot formation [1,3]. However, a rather large sheet density is necessary to achieve an appreciable recombination rate, in agreement with the rather high threshold sheet density observed in experiments. The transition blue shift has also been observed experimentally [7,8].

We notice further that the blue shift just mentioned is relative to the red-shifted transition energy in the unscreened polarization field. This can be read off Fig. 4, displaying transition energies and recombination rate vs well width. At low sheet densities, the transition energy suffers a linear red shift for increasing well width. The transition energy becomes insensitive to well width (saturating to about  $3 \text{ eV}$  above  $50 \text{ \AA}$ ) only for sheet densities higher than  $5 \cdot 10^{13} \text{ cm}^{-2}$ . This behavior, also observed experimentally [16], is easily understood by considering again Fig. 1. At low densities, the polarization field is unscreened and the potential drop in the well increases with the well width, thus reducing the energy separation between  $V1$  and  $C1$ . For high sheet densities, the field is screened out over most of the well, with an effective screening length as small as  $\approx 25 \text{ \AA}$ . Since the  $V1$  and  $C1$  eigenfunctions are localized near the interfaces, an increase in well width will not change the transition energy, but will enhance the geometrical separation of electrons and holes, eventually causing a reduction in the recombination rate (Fig. 4). However, such reduction is much smaller than in the unscreened (low sheet density) case observed experimentally [11].

In conclusion, we have shown that free carriers can effectively screen macroscopic polarization fields in nitride quantum wells, resulting in a non-vanishing recombination rate for large wells (contrary to previous claims) in normal laser operation. A rather high sheet density is needed to achieve this conditions. We also explained the red shifts vs well width and blue shifts vs sheet density as resulting from the interplay of free-carrier screening and polarization fields.

VF acknowledges support from the Alexander von Humboldt-Stiftung and from the PAIS program of INFM Section E.

- 
- [1] S Nakamura *et al.*, App. Phys. Lett. **70**, 2753 (1997);
  - [2] S Nakamura *et al.*, App. Phys. Lett. **72**, 2014 (1998); *ibid.* **73**, 832 (1998);
  - [3] M. B. Nardelli, K. Rapcewicz, and J. Bernholc, Appl. Phys. Lett. **71**, 3135 (1997)
  - [4] K. Domen, A. Kuramata, and T. Tanahashi, App. Phys. Lett. **72**, 1359 (1998);
  - [5] W. Fang, and S. L. Chuang, App. Phys. Lett. **67**, 751 (1995)
  - [6] Y. C. Yeo, T. C.Chong, M. F. Li, and W.J. Fan, J. App. Phys. **84**, 1813 (1998)
  - [7] S. Chichibu, T. Azuhata, T. Sota, and S. Nakamura, Appl. Phys. Lett. **69**, 4188 (1996).
  - [8] M. Osinski *et al.*, V. A. Smagley, J. Crystal Growth **189/190**, 803 (1998)
  - [9] F. Bernardini, V. Fiorentini, and D. Vanderbilt, Phys. Rev. B **56**, R10024 (1997).
  - [10] F. Bernardini and V. Fiorentini, Phys. Rev. B **57**, R9427 (1997); to be published.
  - [11] Jin Seo Im *et al.*, Phys. Rev. B **57**, R9435 (1998)
  - [12] T. Honda *et al.*, J. Crystal Growth **189/190**, 644 (1998)
  - [13] A. Di Carlo *et al.*, Solid State Communications **98**, 803 (1996); A. Di Carlo, MRS Proc. **491** 389 (1998);
  - [14] J-M. Jancu, R. Scholz, F. Beltram, and F. Bassani, Phys. Rev. B **57**, 6493 (1998); R. Scholz, J-M. Jancu, and F. Bassani, MRS Proc. **491** 383 (1998).
  - [15] We use this envelope-function-like picture (which can be relaxed in the tight-binding scheme, see M. Graf and P. Vogl, Phys. Rev. B **51**, 4940 (1995)) in order to make contact with non-self-consistent data [3].
  - [16] T. Takeuchi *et al.*, Jpn. J. Appl. Phys. **36**, L382 (1997).

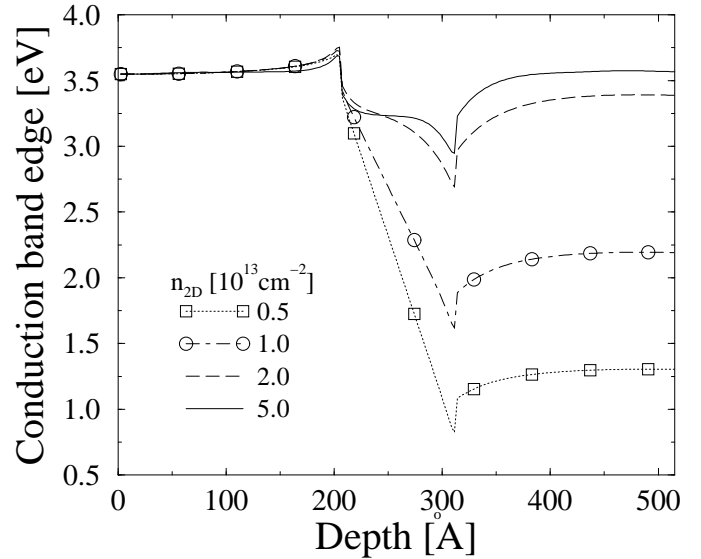


FIG. 1. Conduction band edge profile of a 100 Å InGaN quantum well for several sheet densities

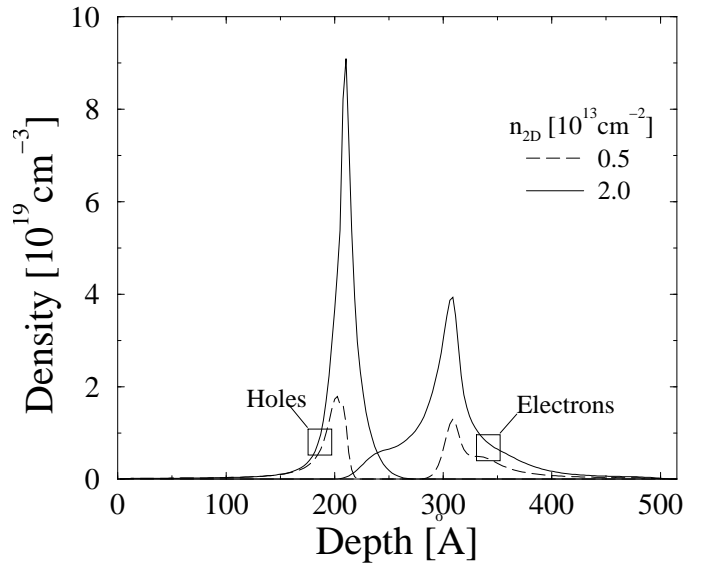


FIG. 2. Electron and hole density of the 100 Å well.

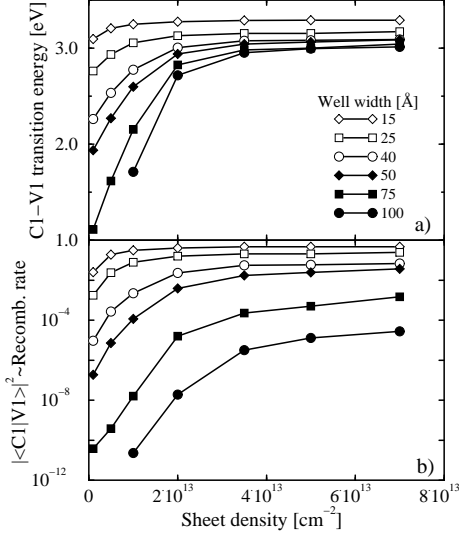


FIG. 3.  $C1-V1$  transition energy and recombination rate vs sheet density for several well widths.

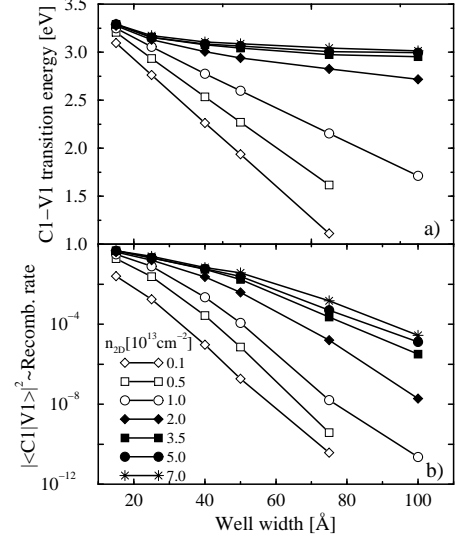


FIG. 4.  $C1-V1$  transition energy and recombination rate vs well width for several densities.

Parameter	GaN	$\text{In}_{0.2}\text{Ga}_{0.8}\text{N}$
$E_g$ [eV]	3.548	3.157
$e_{31}$ [C/m <sup>2</sup> ]	-0.49	-0.51
$e_{33}$ [C/m <sup>2</sup> ]	0.73	0.77
$C_{13}$ [GPa]	108	105
$C_{33}$ [GPa]	399	359
$P_s$ [C/m <sup>2</sup> ]	-0.0290	-0.0296
$\varepsilon_r$	10.28	11.15

TABLE I. Parameters used in this work.